

# Effect of Co doping on the physical properties of Sn<sub>2</sub>S<sub>3</sub> thin film

A. Mary Saroja<sup>1</sup> · I. Kartharinal Punithavathy<sup>2</sup> · S. Johnson Jeyakumar<sup>2</sup> ·  
A. R. Balu<sup>3</sup> · S. Joshua Gnanamuthu<sup>2</sup>

Received: 4 January 2017 / Accepted: 10 April 2017 / Published online: 19 April 2017  
© Springer Science+Business Media New York 2017

**Abstract** Cobalt doped Sn<sub>2</sub>S<sub>3</sub> thin films with a dopant concentration of 1, 2 and 3 at. wt% have been coated on glass substrate by spray pyrolysis method and the structural, optical, electrical and magnetic properties of the film investigated. XRD pattern confirms the polycrystalline nature of the films and the preferential orientation of the crystal is along the (211) direction. The band gap energy of the undoped film is 1.77 eV and can be tailored by the addition of Co atoms. The absorption coefficient of all the films is of the order of 10<sup>4</sup> Ωcm<sup>-1</sup> near the fundamental absorption edge and is very much suitable for photovoltaic applications. The electrical conductivity increases due to cobalt addition and is maximum for a concentration of 2 wt%. The presence of Cobalt in Sn<sub>2</sub>S<sub>3</sub> thin film introduces ferromagnetic properties even at room temperature. Addition of Cobalt in Sn<sub>2</sub>S<sub>3</sub> has improved its optical and electrical properties and also paved the way for its use as a dilute magnetic semiconductor (DMS).

## 1 Introduction

Metal Chalcogenide thin films are of great interest in the field of photo voltaic devices as they contribute to interesting phenomenon on interaction with light. The

chalcogenide Tin sulphide occurs in various phases like SnS, SnS<sub>2</sub>, Sn<sub>2</sub>S<sub>3</sub>, Sn<sub>3</sub>S<sub>4</sub> and Sn<sub>4</sub>S<sub>5</sub> and exhibits coordinating behaviour like all other chalcogenides. Among the various phases of tin sulphide, Sn<sub>2</sub>S<sub>3</sub> is a mixed valence IV–VI chalcogenide compound in which tin has a valence of both II and IV in equal ratios. Sn<sup>II</sup>Sn<sup>IV</sup>S<sub>3</sub> possesses tetrahedral chain coordination between Sn<sup>II</sup> and S and alternatively octahedral chain coordination between Sn<sup>IV</sup> and S forming an orthorhombic P<sub>nma</sub> structure and each unit cell contains four Sn(II) atoms, four Sn(IV) atoms and twelve Sulphur atoms [1]. The Sn(II) state has only two electrons bonded to S resulting in a lone pair of electron which gives rise to a distorted octahedral. This structure results in Sn<sub>2</sub>S<sub>3</sub> behave as a semiconductor in spite of the usual insulating behaviour of other type I mixed valence compounds. It has a direct band gap ranging from 0.85 to 2.2 eV [2, 3] and absorption coefficient of the order of 10<sup>4</sup> cm<sup>-1</sup> in the visible region and hence is a suitable absorber layer for photovoltaic devices. Sn<sub>2</sub>S<sub>3</sub> thin film has been prepared successfully by various methods like chemical bath deposition, electro deposition, spray pyrolysis and co-evaporation [4–7].

Doping of semiconductors is very essential for electronic and optoelectronic applications. Efforts to dope II–VI semiconductors (CdTe, ZnSe, CdSe, ZnO), III–V semiconductors (GaN, GaAs), and quaternary semiconductors (CIGS, CZTS) with transition metal ions have been studied and are found to possess a combination of both charge and spin related properties which can be exploited for promising applications. Transition metal doped semiconductors find potential application in energy transfer and sensing, light emitting diodes, optoelectronic devices, data storage etc., [8]. Transition metal doped TiO<sub>2</sub> also find application in photo electrochemical cells as anodes and are used to split water thereby generating hydrogen which is an excellent source of energy. The transition metals serve as

✉ A. Mary Saroja  
saro.kumarjj@gmail.com

<sup>1</sup> Department of Physics, Bharathiyar College of Engineering & Technology, Karaikal, Puducherry 609 609, India

<sup>2</sup> Department of Physics, TBML College, Poraiyar, Tamilnadu 609 307, India

<sup>3</sup> Department of Physics, AVVM Sri Pushpam College, Poondi, Tamilnadu 613 503, India

photo catalyst and enhance the utilization of the solar spectrum by tuning the band gap of  $\text{TiO}_2$ . The photo catalytic action of Co and other metal loaded  $\text{TiO}_2$  in improving the stability and efficiency of the photo electrochemical cell has been reported by Momeni et al. [9, 10]. The transition impurity atoms in semiconductors have also given rise to a new class of materials called DMS and paved the way for spin electronic devices. The magnetic property of thin film semiconductors is very much dependent on the concentration of dopants and Cobalt doped samples like Co: CdTe [11], Co: ZnO [12], Co:  $\text{Cu}_2\text{O}$  [13] have shown an appreciable magnetization even for very low doping concentrations. The Co ion has a radius of 0.58 Å which is much less than the radii of  $\text{Sn}^{2+}$  (0.93 Å) as well as  $\text{Sn}^{4+}$  ion (0.61 Å) and so can diffuse well into the lattice of  $\text{Sn}_2\text{S}_3$ . Doping of cobalt ions can result mostly in substitution of  $\text{Sn}^{2+}$  or  $\text{Sn}^{4+}$  ions and also to some extent incorporation at the interstitial sites between the host atoms. Cobalt has a charge of  $\text{Co}^{2+}$  or  $\text{Co}^{3+}$  and hence can improve the conductivity and being ferromagnetic will lead to the formation of Co:  $\text{Sn}_2\text{S}_3$  transparent magnetic semiconductor. In this paper an effort to improve the surface morphology, crystal structure, band gap and magnetic properties of  $\text{Sn}_2\text{S}_3$  absorber layer by doping with the ferromagnetic transition metal cobalt for photovoltaic and magnetic applications has been investigated by spray pyrolysis technique. Spray pyrolysis technique leads to the synthesis of Nano needle structured  $\text{Sn}_2\text{S}_3$  thin films which limit the particle boundaries thereby reducing the recombination of electron and holes resulting in enhanced electrical conductivity.

### 1.1 Experimental details

Spray Pyrolysis is a non-vacuum method of depositing thin film and hence is a less expensive and simple technique which does not involve complex processes for deposition. Dopant addition requires just the solubility of the dopant in precursor solution and is very easily carried out in this method. Spray pyrolysis deposition of  $\text{Sn}_2\text{S}_3$  thin films on glass substrates have been successfully done at an optimized molar concentration [14] and for a spray volume of 30 ml [15] and a black shining transparent thin film of  $\text{Sn}_2\text{S}_3$  was uniformly coated. The base cationic solution consists of 0.025 M of  $\text{SnCl}_2$ ,  $\text{H}_2\text{O}$  and anionic solution is 0.025 M of thiourea CS  $(\text{NH}_2)_2$  both prepared separately in DM water. To increase the solubility of Sn few drops of HCl is added to the  $\text{SnCl}_2$  precursor solution. Both the cationic and anionic base solution is mixed in equal ratios to obtain a homogenous precursor solution. Co ions of concentrations 1, 2 and 3 at. wt% with respect to Sn are added to the base cationic solution by dissolving Cobalt(II) chloride of appropriate amount. The precursor solution was sprayed using an atomizer on to ultrasonically cleaned glass plates maintained at a substrate temperature of 400 °C [16]. A

schematic representation of the preparation of the precursor solution and the experimental set up is shown in Fig. 1.

Structural variations due to dopant addition was determined using X-ray diffractometer (XRD) PAN analytical-PW3050/60 X'Pert PRO with  $\text{CuK}\alpha$  radiation ( $\lambda = 1.5406 \text{ \AA}$ ) X-ray source. The surface morphology of the film was studied using atomic force microscope (Agilent—5500 AFM) and Scanning tunnelling microscope (HITACHI S-3000H). The thickness of the film depends on the concentration of the dopants and is measured using stylus Profilometer (SJ-301). The concentration of the different elements in the film was analysed with EDX BRUKER analyser. The band gap of the film was determined from the optical data obtained using UV-Vis-NIR double beam spectrophotometer (JASCO V-670) in the wavelength range 200–1200 nm. Photoluminescence (PL) spectra were studied using Varian Cary Eclipse Photoluminescence spectrophotometer. Electrical measurements were carried out using Keithley SCS 4200 semiconductor characterization system. The influence of magnetic properties in the presence of dopants was measured using Cryogenic mini VSM 3639.

## 2 Results and discussions

### 2.1 Structural properties

The XRD pattern of all the films show a strong peak corresponding to the plane (211) and also a weak one for the plane (422) as seen in Fig. 2. There are no peaks related to other sulphides of tin like SnS or  $\text{SnS}_2$  and the XRD results agree very well with JCPDS card No. 75-2183 indicating that the obtained films are polycrystalline with orthorhombic structure and the preferred orientation is along (211) which agrees with that reported by Khadroui et al. [6] The intensity of the XRD peak is much reduced for the doped films when compared to the undoped and this is due to the incorporation of the smaller  $\text{Co}^{2+}$  ions (0.58 Å) at the larger  $\text{Sn}^{2+}$  (0.93 Å) cationic site which causes internal stress in the crystal lattice without appreciable change in the crystal structure. Among the doped films the crystallinity of the film is enhanced for a dopant concentration of 2 wt% and thereafter for further increase in dopant concentration, the crystallinity decreases.

The size of the crystal (D) is calculated from the Scherrer formula

$$D = \frac{0.9\lambda}{\beta \cos \theta} \quad (1)$$

where (D) is the average grain size,  $\lambda = 1.542 \text{ \AA}$  is the X-ray wave-length, ( $\beta$ ) is the full width at half maximum (FWHM) of XRD peaks and ( $\theta$ ) is the diffraction angle.

The micro strain ( $\epsilon$ ) in the film is given by the equation

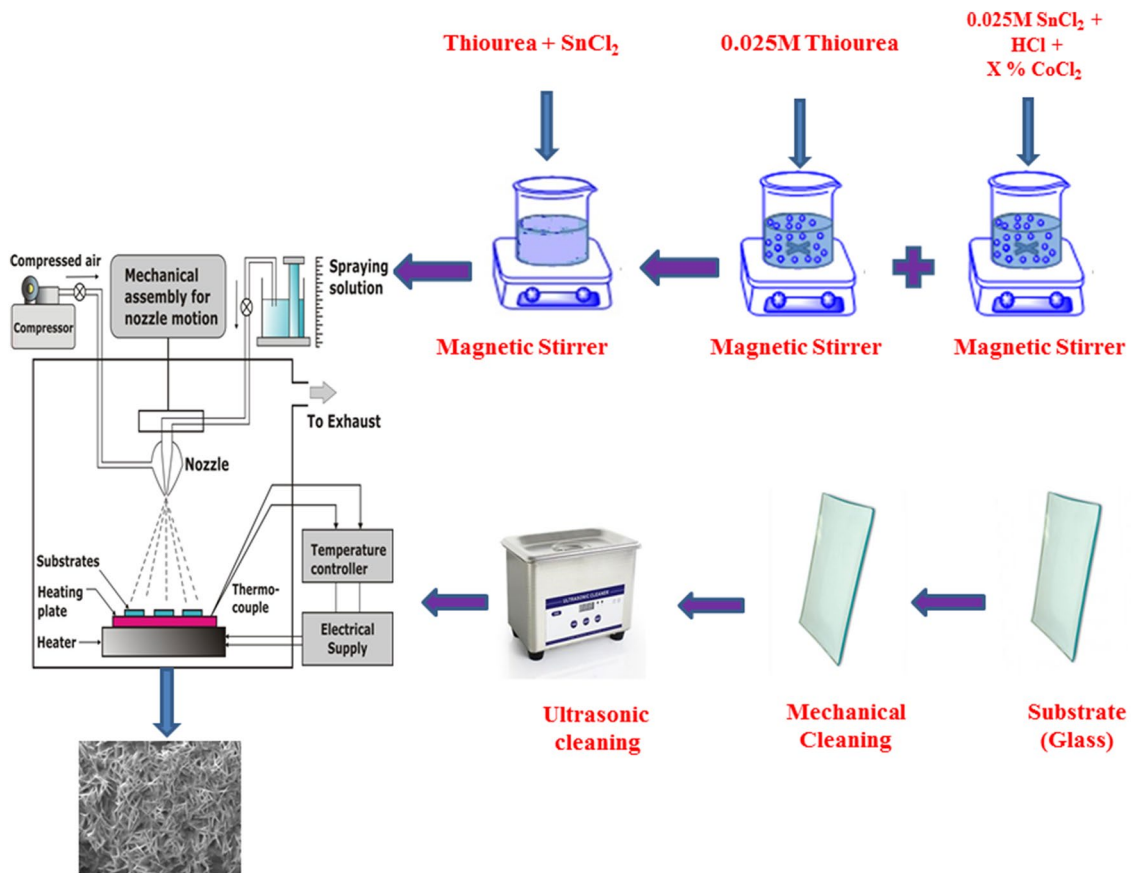


**Fig. 1** Schematic representation of the experimental details of spray deposition of  $\text{Sn}_2\text{S}_3$  thin films on glass substrate

$$\varepsilon = \frac{\beta \cos \theta}{4} \quad (2)$$

and the dislocation density ( $\delta$ ) is calculated from the relation

$$\delta = \frac{1}{D^2} \text{ lines/m}^2 \quad (3)$$

The crystallite size is very much reduced compared to the undoped film and this confirms the substitution of the smaller  $\text{Co}^{2+}$  ion at the larger  $\text{Sn}^{2+}$  ionic site. The crystallite size for the undoped film is  $43.8 \text{ \AA}$  and there is a drastic reduction in crystal size to  $29.2 \text{ \AA}$  at 2 wt% dopant additions and thereafter an increase in crystallite size to  $35.0 \text{ \AA}$  is observed for 3 wt% Co additions. The decrease in crystal size can be explained on the basis of Vegard's law [17] wherein the substitutional atoms (Co) of radii smaller than the host ( $\text{Sn}^{\text{II}}$ ) atoms result in uniform contraction of the crystal and is proportional to the concentration of dopant atoms. Smaller grain size leads to a lesser recombination speed at the grain boundaries as the barrier height is small. Weiner et al., has observed that thin film solar cells with smaller grain size and grown at lower temperatures

(<500°C) have larger  $V_{oc}$  (open circuit voltage) thereby increasing the efficiency of the cell [18]. The increase in crystal size for higher doping concentration of 3 wt% may be attributed to the agglomeration of Co clusters which do not substitute the  $\text{Sn}^{2+}$  ions [19] or may be due to the preferential occupation of interstitial sites at higher concentration [20]. The contraction of the crystal up to a concentration of 2 wt% and expansion of the crystal for 3 wt% is also confirmed by a very small shift of the XRD peak towards the lower diffraction angle and then towards higher angle for 3 wt% for the plane (211). The addition of cobalt atoms increases the lattice defects and thereby an increase in strain is observed compared to the undoped film. The strain is more when the Co atoms occupy the regular cationic sites when compared to the interstitial sites and the structural parameters are given in Table 1. The reduction in crystal size leads to larger surface to volume ratio which influences the structural and optical properties of the film.

The electron micrographs of undoped and Co doped  $\text{Sn}_2\text{S}_3$  films at different concentrations for the same enlargement of  $3 \mu\text{m}$  is shown in Fig. 3a–d. Sharp Nano needle shaped grains densely packed and uniformly distributed without any voids or cracks could be observed for 2 wt%

**Fig. 2** XRD pattern of undoped and Co doped Sn<sub>2</sub>S<sub>3</sub> thin films

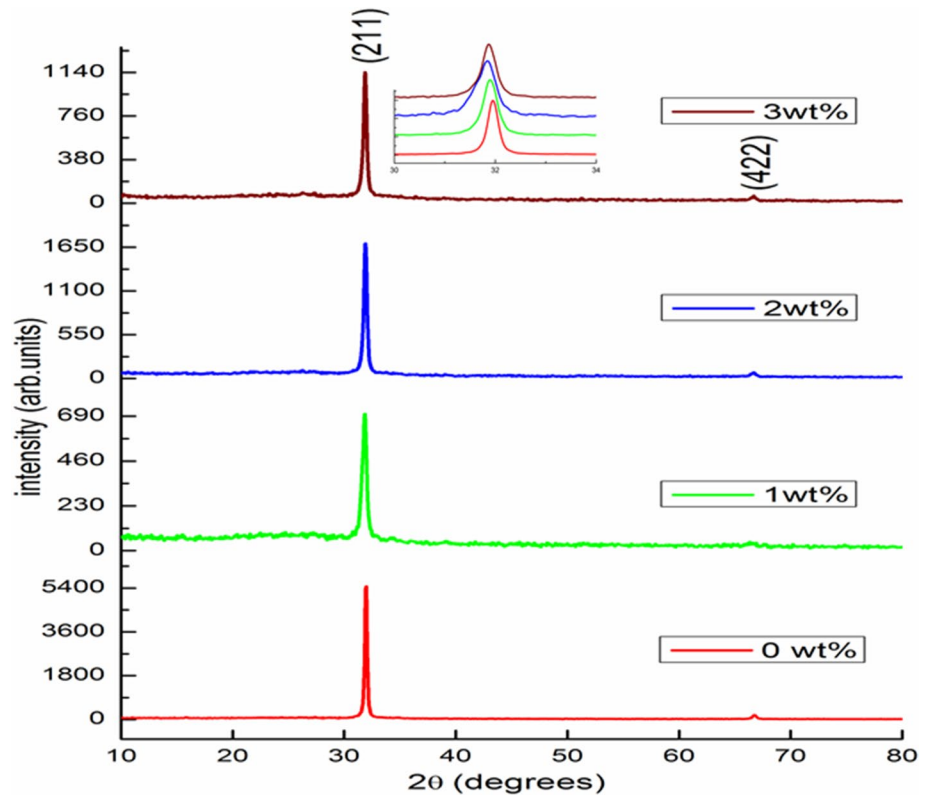


**Table 1** Structural parameters of both undoped and doped Sn<sub>2</sub>S<sub>3</sub> thin films

S.No.	Sample	Inter planar distance d (Å)	FWHM β (radian)	2θ (radian)	Thickness T (μm)	Crystal size (nm)	Dislocation density δ x 10 <sup>15</sup> lines/m <sup>2</sup>	Micro strain ξ x 10 <sup>-4</sup>
1	Undoped	2.8005	0.1968	31.9580	2.04	43.8	0.52	8.26
2	1 wt%	2.8046	0.2952	31.9106	1.35	29.24	1.17	12.38
3	2 wt%	2.8086	0.2952	31.8633	0.91	29.23	1.15	12.39
4	3 wt%	2.8069	0.2460	31.8824	0.89	35.08	0.81	10.32

Co doping. The surface appears to be uneven with the presence of both sharp needle structures as well as diffused and flattened needles for the concentration of 1 and 3 Wt% Co concentrations. The AFM 3D micrograph of Sn<sub>2</sub>S<sub>3</sub> thin film for the dopant concentration of 2 wt% has been recorded and shown in Fig. 4. The AFM results are in good agreement with the SEM images. The substrate is uniformly covered with a dense packing of Nano needles and the average roughness of the surface is 122 nm. The Energy Dispersive X-ray (EDX) spectrum confirms the presence of S, Sn and Co in the film and there is deviation in elemental composition of Sn and S from stoichiometry and is shown in Fig. 5. The atomic weight % of all elements is given in Table 2. It can be observed from EDX that the atomic wt% of Co in the film is almost the same as that in the precursor solution. The ratio of Sn/Co is least for 2 wt% Co addition indicating

the effective replacement of Sn atoms by Co at this concentration and the atomic weight per cent at this concentration is much closer to stoichiometry.

### 2.2 Optical properties

The optical properties of a thin film play a major role for application in electronics and were studied from the transmission spectra obtained over a wavelength range of 200–1200 nm at room temperature. Due to the change in grating element around 900 nm wavelength, there is a slight irregularity in the spectrum. The transparency of the film decreased with increase in Co addition and is observed to be less than the undoped film Fig. 6. This may be due to the reduction in crystallite size as this increases the scattering of incident light and also due to the decrease in crystallinity

**Fig. 3** SEM images of 0,1,2,3 wt% Co doped  $\text{Sn}_2\text{S}_3$  thin films

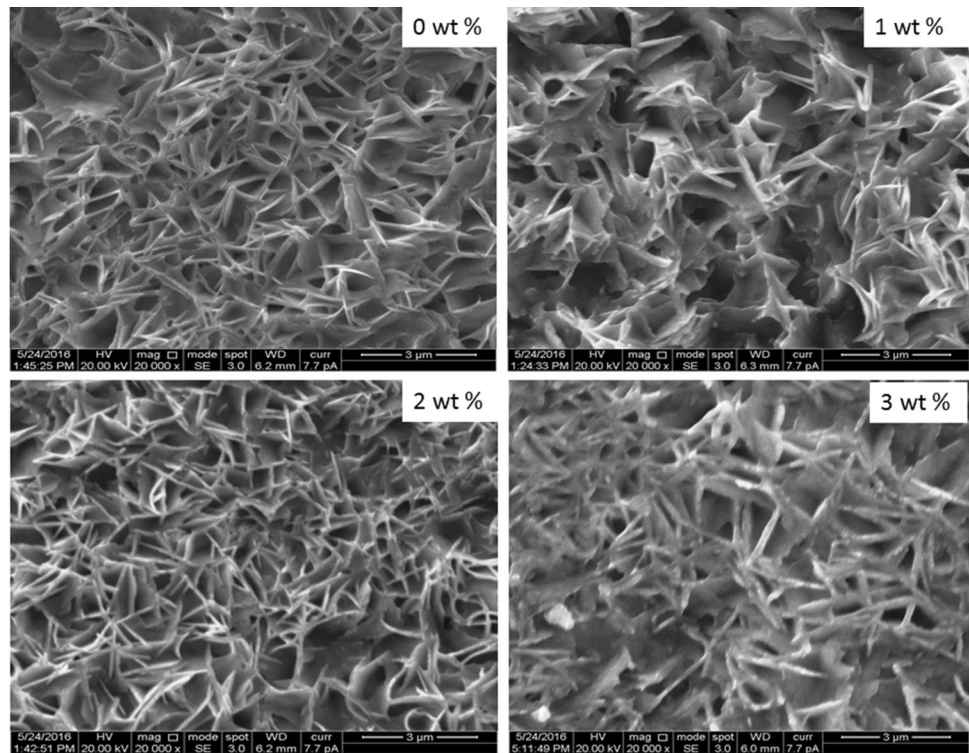
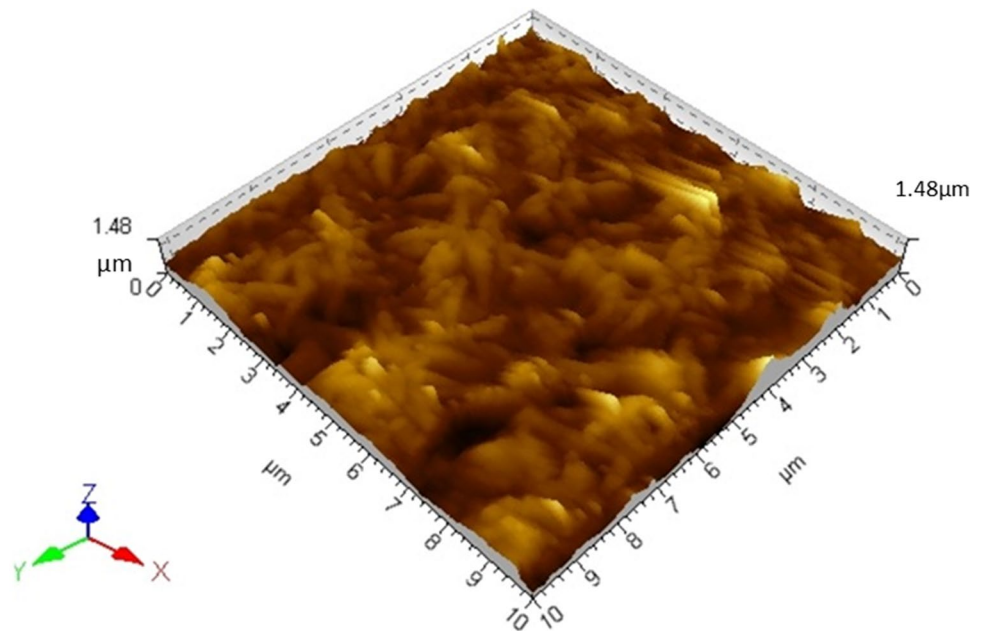


**Fig. 4** AFM images of 2 wt% Co doped  $\text{Sn}_2\text{S}_3$  thin films



of the film. With increase in Co concentration, the Sn/Co ratio decreases increasing the carrier concentration and this may also give rise to a decrease in transmittance. The absorption coefficient ( $\alpha$ ) for all the films is of the order of  $10^4 \text{ cm}^{-1}$  and is almost a constant over the entire visible range. The absorption coefficient increases with increase in Co concentration and is calculated using the formula.

$$\alpha = \frac{1}{t} \ln \frac{1}{T} \quad (4)$$

where  $t$  is the thickness of the film and  $T$  is the transmittance.

The band gap for direct allowed transitions is determined using the relation

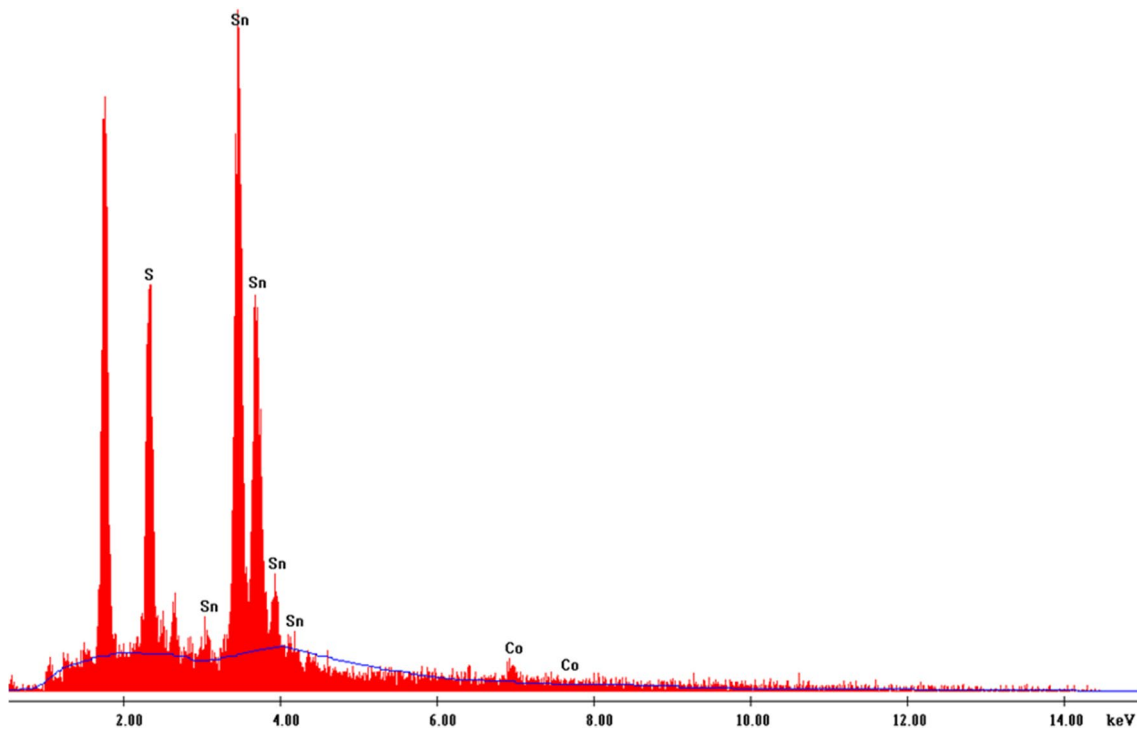


Fig. 5 EDX analysis of 2 wt% Co doped Sn<sub>2</sub>S<sub>3</sub> thin films

Table 2 Elemental composition, electrical and optical data at different Co concentrations of Sn<sub>2</sub>S<sub>3</sub> thin films

S.No.	Dopant concentration	Sn Atomic wt%	S Atomic wt%	Co Atomic wt%	Sn/Co	Conductivity (Ωcm) <sup>-1</sup>	Urbach’s energy E <sub>U</sub> (eV)	Band gap energy E <sub>g</sub> (eV)
1	0%	61.99	38.01	–	–	0.26	0.26	1.80
2	1%	61.33	34.91	3.76	16.31	0.74	0.35	1.72
3	2%	60.68	32.87	6.45	9.40	1.35	0.58	1.69
4	3%	61.49	33.77	4.74	12.97	1.33	0.78	1.62

$$(\alpha h\nu) = A(h\nu - E_g)^{1/2} \tag{5}$$

where h is Planck’s constant, ν is the frequency of the incident photon, A is the band edge sharpness constant and E<sub>g</sub> is the band gap. The direct band gap energies for all the films were obtained from the (αhν)<sup>2</sup> versus (hν) curve by extrapolating the linear portion of the Tauc plot and finding the energy corresponding to the zero absorption coefficient. The band gap is found to decrease with increase in Co concentration and is 1.80, 1.72, and 1.69, 1.62 eV for undoped, 1, 2 and 3 wt% concentrations respectively as shown in Fig. 6 (inset). The observed band gap energies are consistent with that reported by Joshua et al. [21] except for a very small deviation due to different deposition conditions. The red shift is very much expected as the dopant Co atoms give rise to shallow energy levels near the valence band edge.

Thus with increase in dopant concentration the density of energy states increase giving rise to a continuum (Urbach’s tail) and this decreases the band gap. The Urbach’s energy (E<sub>U</sub>) is tabulated in Table 2 and is calculated from the slope of the graph between ln α and hν where

$$\alpha = \alpha_0 \exp \frac{h\nu}{E_U} \tag{6}$$

and the intercept of the graph is a measure of the constant α<sub>0</sub>. The decrease in band gap energy also substantiates the substitution of Sn cationic sites by Co<sup>2+</sup> ions and indicates the possibility of tailoring the band gap by Co addition.

The optical quality of the film is best characterised by PL intensity and Fig. 7 shows the Photo Luminescent spectra for both undoped and doped Sn<sub>2</sub>S<sub>3</sub> film. The emission

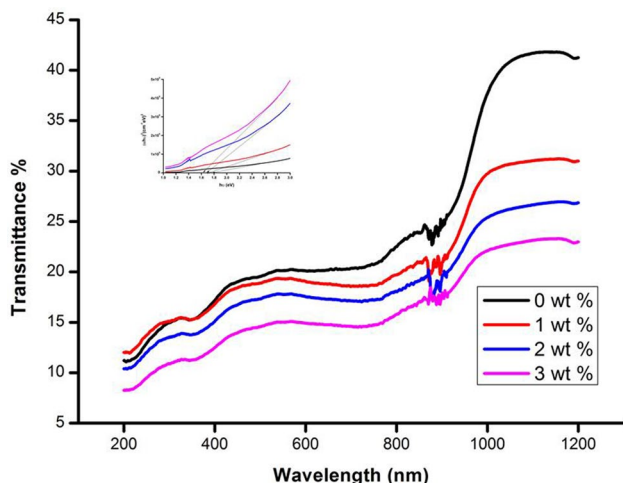


**Fig. 6** Transmittance spectra and Tauc's plot (*inset*) of undoped and Co doped  $\text{Sn}_2\text{S}_3$  thin films

peaks are observed at 520, 495, 442, 377 and 360 nm and the intensity of the peaks are enhanced due to cobalt addition confirming the increase in the number of vacancies. Higher concentration of defects, higher recombination rate and reduction in crystalline nature increases the intensity of PL peaks. Due to the volatile nature of Sulphur, vacancies are created and in addition to that  $\text{Co}^{2+}$  ions occupying  $\text{Sn}^{4+}$  positions also create sulphur vacancies and this gives rise to the peak observed at 360 and 370 nm [22]. The PL peak at 440 nm wavelength may be attributed to the transition of electrons from the edge of conduction band to the holes trapped at the surface states present in the energy band gap and the peak at 520 nm corresponds to the band edge emission [23]. The peak around 495 nm may be due to impurity bound exciton [24].

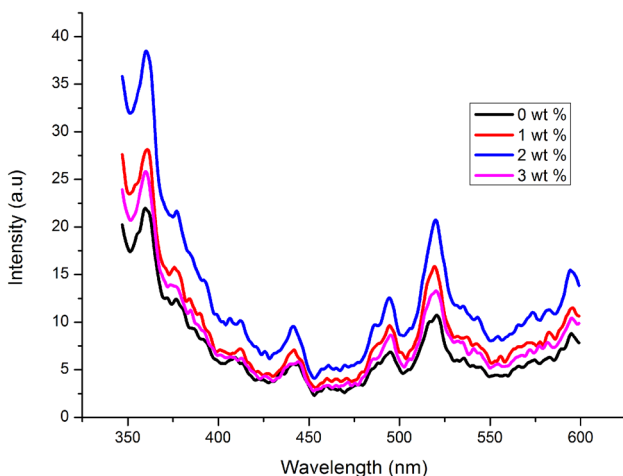


**Fig. 7** PL spectra of Co doped  $\text{Sn}_2\text{S}_3$  thin films

### 2.3 Electrical properties

The electrical studies on the  $\text{Sn}_2\text{S}_3$  thin film has been investigated with the help of Keithley instrument and the conductivity of the film is determined from the I-V graph and reported in Table 2. The conductivity of the Co doped films increase with Co addition and has a maximum value of  $1.35 (\Omega\text{cm})^{-1}$  at 2 wt% concentration. There after the conductivity decreases on further increase in dopant concentration as shown in Fig. 8 and this can be attributed to the increase in carrier concentration on the addition of dopants. With increase in concentration of dopants up to 2 wt% the  $\text{Sn}^{2+}$  ions are replaced not only by isovalent substitution but also by the other valence states like  $\text{Co}^{3+}$  leading to an increase in carrier concentration and this results in increase in conductivity [25]. The  $\text{Co}^{2+}$  occupying the  $\text{Sn}^{4+}$  sites lead to sulphur vacancy which would generate two electrons for every Co addition thereby increasing the carrier concentration.  $\text{Sn}_2\text{S}_3$  will be either n or p type depending on the domination of S or Sn vacancy respectively. For 3 wt% dopant addition the Co atoms being smaller in size compared to Sn occupy the interstitial sites and there is a decrease in conductivity. Co addition of 2 wt% increases the conductivity of the thin film and will contribute in enhancing the performance of the photovoltaic.

### 2.4 Magnetic properties

The magnetic properties of undoped and transition metal doped  $\text{Sn}_2\text{S}_3$  thin films were investigated by plotting the Magnetic moment versus Magnetic field (m-H) curve at room temperature as shown in Fig. 9. The diamagnetic behaviour of  $\text{Sn}_2\text{S}_3$  is clearly understood from the negative slope of the m-H curve with contribution from the glass substrate also. A reversal of magnetization sets in with the

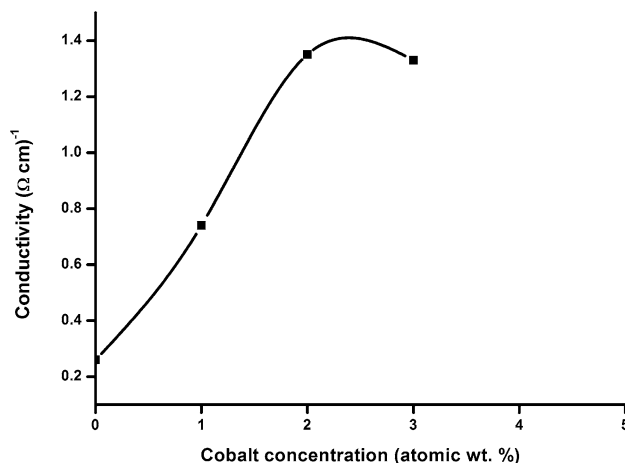


**Fig. 8** Electrical conductivity of  $\text{Sn}_2\text{S}_3$  thin films with different Co concentration

introduction of Co ions and a well-defined hysteresis loop is obtained for 2 wt% concentrations confirming their ferromagnetic behaviour at room temperature. The paramagnetic behaviour is observed to a minimal extent for 1 at. wt% concentration. The enhancement of ferromagnetism at 2 wt% concentration can be attributed to the small crystallite size [26], increase in dopant concentration and the presence of defects. As the concentration of transition metal is increased it leads to an increase in defects mainly sulphur vacancy which is understood from the enhanced peaks observed in the PL graph and the increase in electrical conductivity. This contributes to the strong exchange interaction between the d orbitals of the Co ions and the orbitals of the trapped electrons in the sulphur vacancy. The reduction in crystallite size at 2 wt% is also inferred from the XRD analysis. On further increasing the Co concentration a reduction in ferromagnetic behaviour is observed and this may be attributed to the cluster formation which results in decreased Co–Co distance contributing to the antiferromagnetic coupling between them [27].

## 2.5 Conclusion

Spray pyrolysis deposition of undoped and Cobalt doped  $\text{Sn}_2\text{S}_3$  thin films have been experimented on glass substrates and the influence of Co on the structural, optical, electrical and magnetic properties investigated. Co doped  $\text{Sn}_2\text{S}_3$  thin films with Nano needle structures were uniformly coated for a dopant concentration of 2 wt%. The doped films were transparent with an absorption coefficient of  $10^4 \text{ cm}^{-1}$  in the visible region. XRD analysis confirms the deposition of single phase  $\text{Sn}_2\text{S}_3$  orthorhombic crystals. The band gap of the films decreased from 1.80 to 1.62 eV on dopant addition indicating the possibility of tuning the band gap

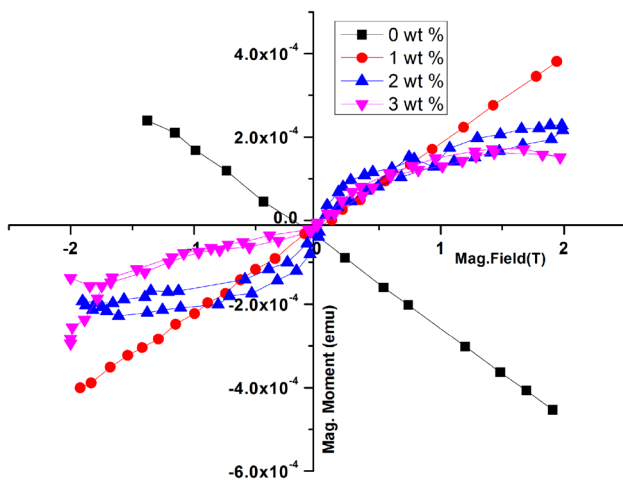


**Fig. 9** Plot of Magnetic moment versus Magnetic field of undoped and Co doped  $\text{Sn}_2\text{S}_3$  thin films

by Co addition. The electrical conductivity of the 2 wt% Co doped film was found to be maximum with conductivity  $1.35 (\Omega\text{cm})^{-1}$ . The optical and electrical data obtained for 2 wt% Co doped  $\text{Sn}_2\text{S}_3$  confirms its application as an absorber layer in photo voltaic cells. Magnetic studies have revealed the presence of ferromagnetism in Co doped  $\text{Sn}_2\text{S}_3$  thin films at room temperature and suggests the possibility of altering the magnetic characteristics by Co addition.

**Acknowledgements** The authors are thankful to the Head, Department of Physics and Mr. Karthik, Technical Assistant, Alagappa University, Karaikudi for XRD analysis and magnetic studies.

## References

1. R. Kniep, D. Mootz, U. Severin, H. Wtjnderlich, *Acta cryst.* **B38**, 2022 (1982)
2. U. Alpen, J. Fenner, E. Gmelin, *Mat. Res. Bull.* **10**, 175 (1975)
3. H.B. Salah, H. Bouzouita, B. Rezig, *Thin Solid Films* **480**, 439 (2005)
4. E. Güneri, F. Göde, B. Boyarbay, C. Gümüş, *Mat. Res. Bull.* **47**, 3738 (2012)
5. B. Chen, X. Xu, F. Wang, J. Liu, J. Ji, *Mater. Lett* **65**, 400 (2011)
6. M. Khadraoui, N. Benramdane, C. Mathieu, A. Bouzidi, R. Miloua, Z. Kejjaba, K. Sahraoui, R. Desfeux, *Sol. State. Commun.* **150**, 297 (2010)
7. T.S. Reddy, M.S. Kumar, *Ceram. Int.* **42**, 12262 (2016)
8. S.J. Pearton, C.R. Abernathy, D.P. Norton et al., *Mater. Sci. Eng.* **40**(4), 137 (2003)
9. M.M. Momeni, Y. Ghayeb, *Ceram. Int.* **42**, 7014 (2016)
10. M.M. Momeni, Y. Ghayeb, *J. Mater. Electron.* **27**, 3318 (2016)
11. M. Rigana Begam, N.M. Rao, G.M. Joshi, S. Kaleemulla, M. Shobana, N. Sai Krishna, M. Kuppan, *Struct. Adv. Condens Matter Phys.* (2013). doi:10.1155/2013/218659
12. S.-L. Ou, H.-R. Liu, S.-Y. Wang, D.-S. Wu, *J. Alloys comp.* **663**, 107 (2016)
13. S.N. Kale, S.B. Ogale, S.R. Shinde, M. Sahasrabudhe, V.N. Kulkarni, *Appl. Phys. Lett.* **82**, 2100 (2003)
14. J. Srivind, V.S. Nagarethinam, A.R. Balu, *Mater. Sci. Poland* **34**(2), 393 (2016). doi:10.1515/msp-2016-0035
15. D. Prabha, S. Ilangovan, V.S. Nagarethinam, A.R. Balu, *Mater. Res. Innov.* **20**(4), 307 (2016). doi:10.1080/14328917.2015.1134854
16. A.M. Saroja, I.K. Punithavathy, S.J. Jeyakumar, S.J. Gnanamuthu, A.R. Balu, *Optik* **130**, 245 (2017)
17. L. Vegard, *Die Konstitution der Mischkristalle und die Raumfüllung der Atome.* *Z. Phys.* **5**, 17 (1921)
18. J. Werner, R. Bergmann, *Technical Digit 12th Int. Photovoltaic Science and Engineering Conf.*, Sapporo, p. 2041 (1999)
19. S. Vijayalakshmi, S. Venkataraj, R. Jayavel, *J. Phys.D. Appl. Phys* **41**, 245403 (2008)
20. A. Nakrela, N. Benramdane, A. Bouzidi, Z. Kejjab, M. Medles, C. Mathieu, *Results Phys.* **6**, 133 (2016)
21. S.J. Gnanamuthu, S.J. Jeyakumar, I.K. Punithavathy, P.J. Prabhakar, M. Suganya, K. Usharani, A.R. Balu, *Optik* **127**, 3999 (2016)
22. S.R. Chalana, R. Vinodkumar, I. Navas, V. Ganesan, V.M. Pillai, *J. Lumin.* **132**, 944 (2012)
23. S. Jana, S. Goswami, S. Nandy, K.K. Chattopadhyay, *J. Alloys Compd.* **481**, 806 (2009)



24. S.J. Gnanamuthu, S.J. Jeyakumar, I.K. Punithavathi, K. Parasuram, V.S. Nagarethinam, A.R. Balu, *Trans. Indian Inst. Met.* doi:[10.1007/s12666-016-0946-0](https://doi.org/10.1007/s12666-016-0946-0)
25. R. Kumaravel, S. Bhuvaneswari, K. Ramamurthi, V. Krishnakumar, *Appl. Phys.A* **109**, 579 (2012)
26. T.R. Cunha, I.M. Costa, R.J.S. Lima, J.G.S. Duque, C.T. Mendes, *J. Supercond. Nov. Magn.* **26**, 2299 (2013)
27. O.D. Jayakumar, H.G. Salunke, R.M. Kadam, M. Mohapatra, G. Yaswant, S.K. Kulshreshtha, *Nanotechnology* **17**, 1278 (2006)